ACS NANO

www.acsnano.org

Article

Chemically Interrogating N-Heterocyclic Carbenes at the Single-Molecule Level Using Tip-Enhanced Raman Spectroscopy

Linfei Li, Sayantan Mahapatra, Jeremy F. Schultz, Xu Zhang, and Nan Jiang*

Cite This: *ACS Nano* 2024, 18, 32118−32125

Read Online

ACCESS | Metrics & More | Article Recommendations | Supporting Information

ABSTRACT: N-heterocyclic carbenes (NHCs) have been established as powerful modifiers to functionalize metal surfaces for a wide variety of energy and nanoelectronic applications. To fundamentally understand and harness NHC modification, it is essential to identify suitable methods to interrogate NHC surface chemistry at the spatial limit. Here, we demonstrate tip-enhanced Raman spectroscopy (TERS) as a promising tool for chemically probing the surface properties of NHCs at the single-molecule scale. We show that with subnanometer resolution, TERS measurements are capable of not only unambiguously identifying the chemical structure of individual NHCs by their vibrational fingerprints but also definitively determining the binding mode of NHCs on metal surfaces. In particular, by investigating low-temperature NHC adsorption on Ag(111), our TERS studies provide insights into the temperature dependence of the adsorption properties of NHCs. This work suggests the potential of single-molecule vibrational spectroscopy for investigations of NHC surface modification at the most fundamental level.

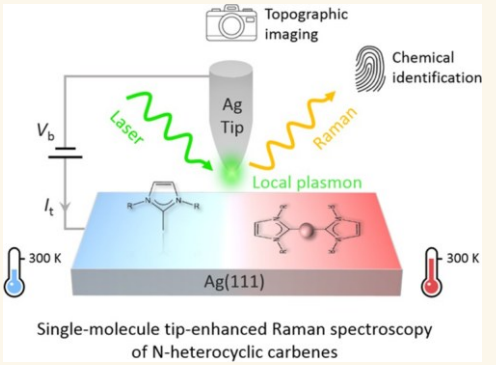

Single-molecule tip-enhanced Raman spectroscopy of N-heterocyclic carbenes

KEYWORDS: *N-heterocyclic carbenes, Raman spectroscopy, TERS, STM, Ag(111)*

INTRODUCTION

Surface modification is a well-established strategy to functionalize metal surfaces for applications in chemistry and nanotechnology. Particularly, significant progress has been made since the ground-breaking discovery of isolated N-heterocyclic carbenes (NHCs).[1−14] As one of the most versatile ligands for metal species, NHCs exhibit exceptional structural diversity and significant chemical and thermal stability, promising to replace thiolate ligands for surface modifications in fields such as heterogeneous catalysis, biosensing, (micro)nanoelectronics, and materials science.[1−4] The realization of many NHC-based technological advances and their full potential requires insight into underlying intrinsic properties and microscopic mechanisms at the single-molecule level. However, such information is critically obscured by ensemble averaging inherent to macroscopic measurements or limited chemical sensitivity in topographic imaging, leading to discrepancies among literatures in the definition of the nature of NHC binding to metals.[7,15−19] Consequently, developing a molecular-scale chemical picture of NHCs, which experimentally necessitates both chemical specificity and spatial resolution, is of eminent importance but remains to be explored. One method to address this uses the plasmon-enhanced Raman effect in the tip−sample junction of scanning tunneling microscopy (STM), that is, tip-enhanced Raman spectroscopy (TERS). TERS couples the chemical specificity of Raman spectroscopy with the spatial resolution of STM,[20−25] allowing the surface chemistry of molecular species to be interrogated on an individual level.[24−29] In particular, TERS proves an ability to address nonplanar (tilted or upright) molecular configurations,[30−32] which are generally ill-defined by common surface imaging approaches.

Here, we used combined TERS, STM, and density functional theory (DFT) to investigate the structure and binding mode of NHCs on Ag(111) at the single-molecule scale. Two model NHC molecules, 1,3-bis(2,6-diisopropylphenyl)imidazol-2-ylidene (IPr) and 1,3-dimethylimidazol-2-ylidene (IMe) were studied (Figure 1a). Although their intramolecular features were obscured in STM topographic images, TERS could identify the chemical nature and

Received: August 9, 2024
Revised: October 6, 2024
Accepted: October 10, 2024
Published: November 11, 2024

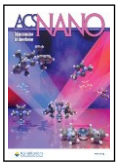

https://doi.org/10.1021/acsnano.4c10942
ACS Nano 2024, 18, 32118−32125

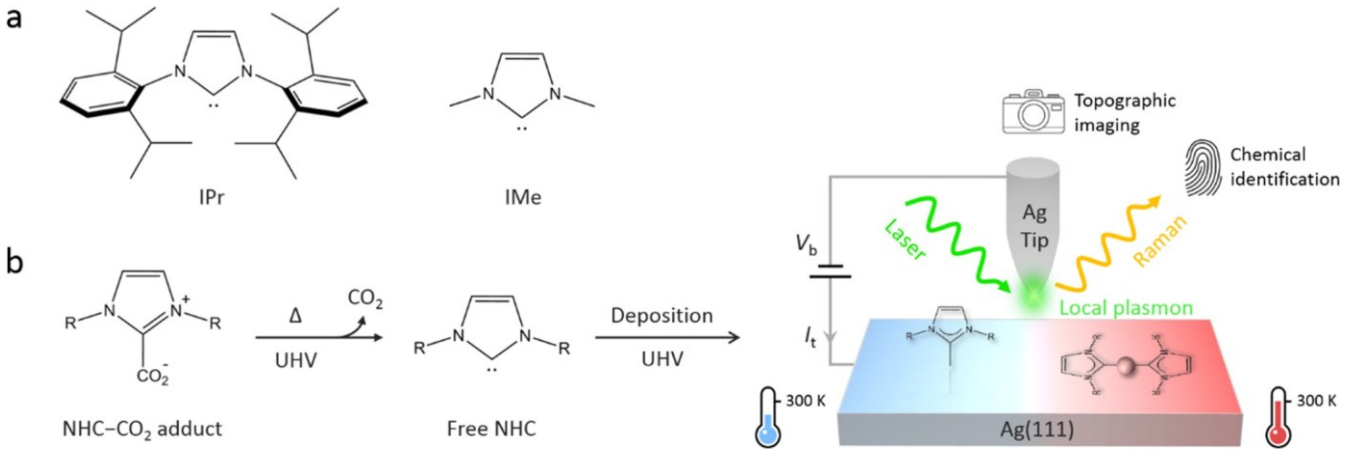

Figure 1. Single-molecule studies of NHCs on Ag(111) using TERS. (a) NHCs used in this study. (b) Schematic of experimental design and setup. UHV: ultrahigh vacuum.

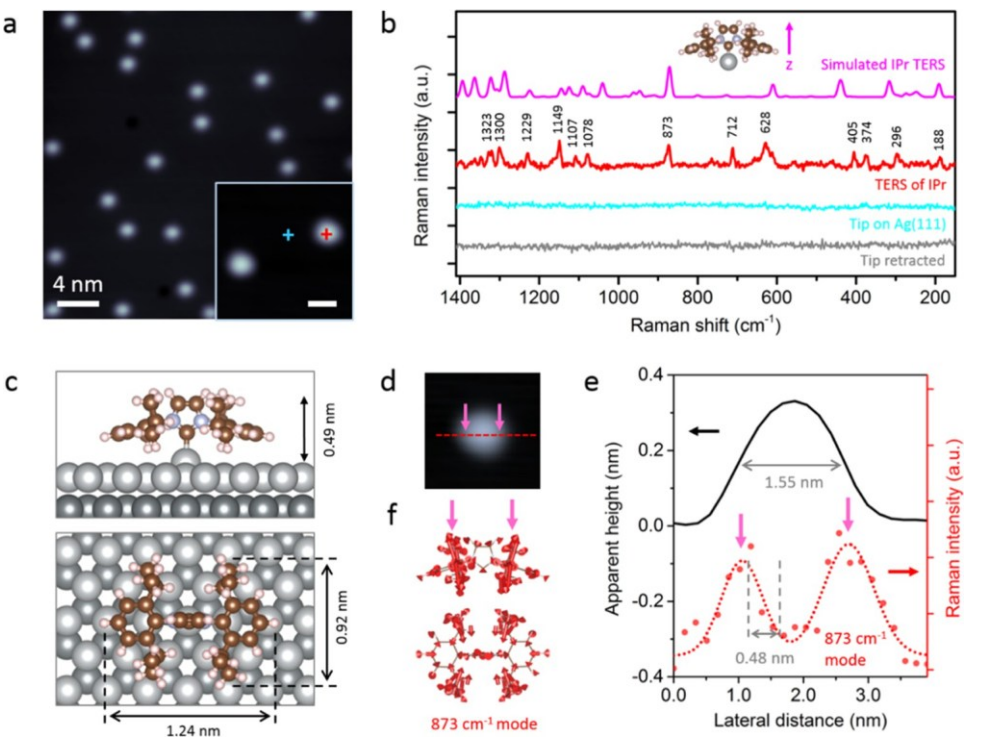

Figure 2. Spectroscopically identifying the structure of single IPr molecules. (a) STM image of LT-deposited IPr on Ag(111). Scale bar (inset): 2 nm. (b) TERS spectra measured at the sites indicated in the inset of (a). For comparison, the simulated TERS spectrum of IPr (magenta) is also shown. (c) Optimized geometry of IPr on Ag(111). (d) STM image of an IPr on Ag(111). Image size: 4.5 nm × 4.5 nm. (e) Height (black) and TERS intensity (red) profiles along the red line in (d). Red dots and curve represent experimental data and Gaussian fit, respectively. (f) Atomic displacements of the 873 cm^{-1} vibrational mode in sectional (top) and plan (bottom) views. Bonded Ag atom is not shown for clarity. STM conditions: (a) 0.7 V, 20 pA; inset: 2.0 V, 30 pA; (d) 2.0 V, 30 pA. TERS parameters: (b) 50 mV, 2 nA, 20 s; (e) 50 mV, 2 nA, 3 s per point with a step length of 0.17 nm.

adsorption geometries of single IPr and IMe by their vibrational signatures with subnanoscale resolution. On this basis, we revealed two distinctly different binding modes of IMe on Ag(111), vertical IMe monomers deposited at low temperature (LT) and flat-lying $(IMe)_2Ag$ complexes formed at room temperature (RT). These results demonstrate the critical role that temperature plays in determining the adsorption properties of NHCs, such as geometry, surface mobility, and self-assembly. In addition to establishing TERS as a promising analytic technique for surface modification, this work offers molecular-level insights into NHC–metal interactions, which contributes to the fundamental understanding of NHC surface properties and the controlled design of new NHC-related functional materials.

RESULTS AND DISCUSSION

Subnanoscale Chemical Identification of Single NHC Molecules. We first show the chemical identification of individual NHCs using TERS. LT deposition of NHCs on Ag(111) was performed following the established procedure (Figure 1b, see details in Methods) to avoid potential molecular self-assembly and intermolecular interactions, thus

https://doi.org/10.1021/acsnano.4c10942
ACS Nano 2024, 18, 32118–32125

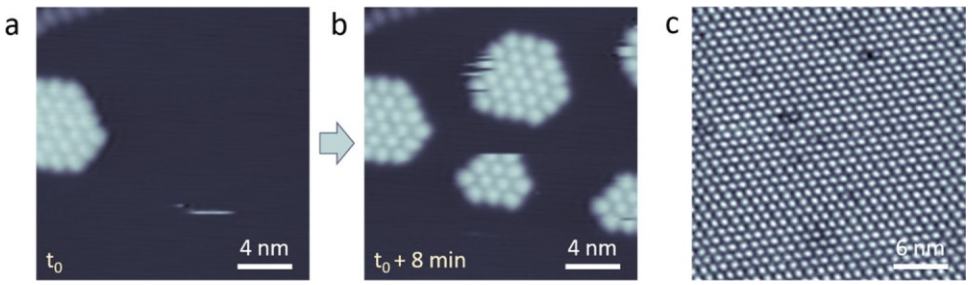

Figure 3. STM topography of IPr on Ag(111) deposited at room temperature. (a, b) Consecutive STM images of RT-deposited IPr acquired 8 min apart on the same area, showing the topographic evolution of self-assembled NHC islands. (c) STM image of full-monolayer IPr molecules on Ag(111). STM conditions: (a) − 2.0 V, 52 pA; (b) − 1.0 V, 52 pA; (c) 1.0 V, 15 pA.

allowing the intrinsic properties of single molecules to be probed. The deposited NHCs on the surface were imaged as stable isolated protrusions (Figure 2a), which conveys very limited information about intramolecular features. More critically, since STM imaging is based on the convolution of topographic and electronic structures, the apparent height and lateral size of NHCs are bias-dependent (Figure S1), preventing the clear identification of NHCs solely by STM topography.

Alternatively, STM-based TERS can circumvent these challenges and identify adsorbed NHCs by detecting their vibrational information at the single-molecule scale. As displayed in Figure 2b, in comparison to the featureless spectrum collected on the bare Ag(111) surface (cyan) or when the tip is retracted from the surface (gray), multiple enhanced Raman peaks (red) are observed when the plasmonically active tip is engaged over a single protrusion (Figure 2a, red plus). This spectral contrast allows us to conclude that the observed Raman peaks result from the species adsorbed on the surface. To elucidate our observations, we performed a TERS simulation using DFT based on an upright free-space IPr that is coupled with a silver atom (Figure S2). Notably, the experimental Raman profile is reproduced well by DFT simulations (Figure 2b, magenta; see mode assignments in Figure S3), thereby identifying the chemical nature of the measured protrusion as a single IPr molecule. Furthermore, due to the surface selection rules of TERS measurements (Figure S4),[33] the relative intensities of vibrational modes in a TERS spectral profile are highly sensitive to variations in the adsorption orientation of a molecule on the surface.[24,28] Consequently, the agreement between experimental and calculated TERS verifies the adsorption geometry of IPr on the surface as illustrated in the inset of Figure 2b, that is, an upstanding adsorption on Ag(111). These observations are further supported by the optimized geometry of IPr on Ag(111) shown in Figure 2c, which consistently reveals an upright binding configuration. Significantly, the IPr covalently binds to a surface Ag atom and pulls it partially out of the Ag(111) lattice (1.13 Å), which is in agreement with the reported adsorption geometry of IPr on Cu(111).[11]

To gain more insight into the chemical structure of single NHCs, we examined the exact evolution of TERS spectra across a single IPr by performing sequential TERS measurements along the line trace marked in Figure 2d. As an example, the intensity profile for the Raman peak at 873 cm^{-1} is presented (Figure 2e, red). The intensity profile exhibits spectral undulation inside the molecule, which is strongest at the molecular edges (magenta arrows) and weakest at the molecular center, providing much finer details compared to the STM height profile (Figure 2e, black) acquired along the same line trace. In fact, on closer inspection the 873 cm^{-1} mode is dominated by vibrations of the isopropyl groups of IPr, whereas those of the center imidazole ring contribute minimally (Figure 2f), which accounts for the depression in the TERS intensity profile. By contrast, the measured 1300 cm^{-1} mode (theoretical 1286 cm^{-1} mode), which is centered on the cyclic ring (Figure S3), peaks in intensity in the middle of the molecule (Figure S5). Moreover, the TERS profile in Figure 2e indicates a chemical spatial resolution of ~0.48 nm (within a 10–90% contrast). Given the measured lateral size of IPr (~1.55 nm), such a high spatial resolution enables the chemistry within an IPr molecule to be resolved.

In addition to low-temperature adsorption, the adsorption of IPr on Ag(111) at room temperature was examined. Instead of isolated single molecules, RT-deposited IPr at submonolayer coverage results in self-assembled close-packed islands on Ag(111) (Figure 3a). These IPr molecules show high mobility on the surface, as demonstrated by varying surface topographies in STM images (Figure 3a,b). These observations are in excellent agreement with the investigation of RT-deposited IPr islands on Au(111).[7] In particular, the formation of IPr–Au adatom complexes on IPr islands was demonstrated by their elevated height (0.24 nm) with respect to single IPr molecules directly bound to the surface. Consistently, the height of RT-deposited IPr islands on Ag(111) (0.45 nm) is measured to be significantly larger than that of LT-deposited single IPr molecules (0.25 nm) (Figure S6), thus demonstrating the presence of Ag adatoms underneath bound to upright IPr molecules on islands. As opposed to stable single IPr molecules directly bonded to Ag(111), the formation of IPr–Ag adatom complexes at room temperature enables IPr to be bound via a mobile adatom to the surface, which accounts for the observed high on-surface mobility. Consequently, highly ordered and hexagonal-dense-packed NHC monolayers are readily achieved upon deposition of IPr at a full coverage, as illustrated in Figure 3c.

Single-Molecule Spectroscopic Determination of the Geometry of NHCs on Ag(111). In addition to identifying the chemical nature of single NHCs, TERS can be used to determine the varied adsorption geometries of an NHC molecule. In contrast to IPr, the large side groups of which force it exclusively into an upright adsorption configuration on coinage metals,[7,11] IMe NHC possesses tiny wingtip groups (methyl, Figure 1a), which is expected to have minimal effect of steric hindrance and thus potentially adopts multiple adsorption geometries on Ag(111). Herein, we first examined LT-deposited IMe on Ag(111), which was found to share

https://doi.org/10.1021/acsnano.4c10942
ACS Nano 2024, 18, 32118–32125

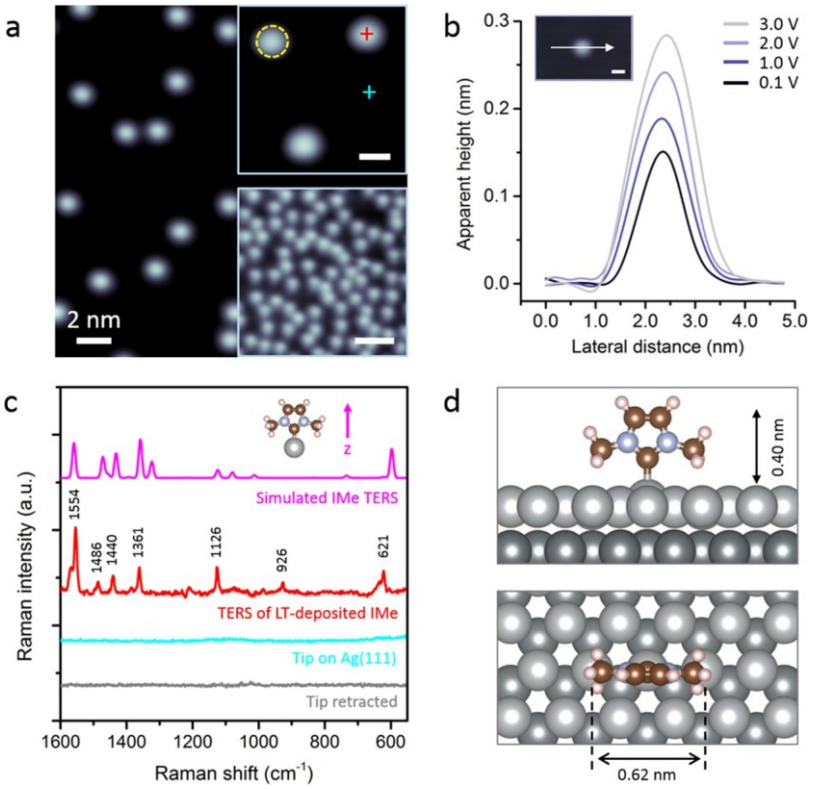

Figure 4. Chemically determining the geometry of IMe on Ag(111) deposited at low temperature. (a) STM topography of LT-deposited IMe on Ag(111). Insets: STM images of low-coverage (top) and high-coverage (bottom) IMe molecules. Scale bars (insets): 1 nm (top) and 4 nm (bottom). (b) Height profiles along the white arrow in the STM image, which was acquired with different biases as indicated. Scale bar: 1 nm. (c) TERS of IMe (red) collected on the molecule indicated in the inset of (a). The simulated TERS spectrum of IMe (magenta) is also shown for comparison. (d) Optimized geometry of IMe on Ag(111). STM conditions: (a) 1.5 V, 30 pA; inset: 2.0 V, 63 pA; (b) 2.0 V, 60 pA. TERS parameters: (c) 30 mV, 2 nA, 15 s.

similar topographic features with IPr, i.e., appearing as stable round protrusions (Figure 4a). Even at high coverage (Figure 4a, bottom inset), LT-deposited IMe on Ag(111) features randomly dispersed single protrusions without complex structures (e.g., dimers and trimers) or self-assembly observed. Although STM imaging offers the primary topographic information, the limited STM resolution and the bias dependence of topographic parameters (Figures 4b and S7) hinder unambiguous identification of the adsorption configuration of IMe on Ag(111).

A TERS measurement was then performed on a single protrusion (Figure 4a, red plus), resulting in a distinct Raman profile (Figure 4c, red). Three important observations can be made. First, this TERS profile is mirrored nicely by the Raman simulation of a free-space IMe coupled with a silver atom as shown in Figure 4c (see mode assignments in Figure S8), thereby corroborating the chemical nature of the measured adsorbate. Second, despite their topographic similarity, the TERS profile observed on IMe significantly differs from the one acquired on IPr (Figure 2b, red), demonstrating the high chemical specificity of TERS. Last and most importantly, the excellent agreement between experimental and calculated TERS demonstrates the molecular orientation on the surface as illustrated in the inset of Figure 4c, that is, a vertical adsorption of IMe on Ag(111).

The above experimental analysis is supported by the calculated geometry of IMe on Ag(111) (Figure 4d). The IMe is found to directly bind to a surface Ag atom at the top site, lifting the bonded atom from its equilibrium position by 0.35 Å. Notably, an IMe–Au adatom complex configuration, where the IMe-bonded surface Au atom is fully pulled out of the surface forming a mobile adatom, has been reported for RT-deposited IMe on Au(111).[7] It is noteworthy that the NHC-induced formation of surface metal adatoms is a thermally activated process in which the free-energy barrier is rather low at RT.[7] However, at temperatures well below RT, e.g., the ones we used here for IMe deposition, there is not enough thermal energy to generate an adatom, leading to a directly bound configuration for LT-deposited IMe on Ag(111) (Figure 4d). This scenario is consistent with the immobility of LT-deposited IMe and the absence of molecular self-assembly on Ag(111) (Figure 4a). The finding that LT-deposited IPr and IMe exhibit the same adsorption properties (e.g., upright geometry and low surface diffusion) regardless of side group structure strikingly highlights the important impact of LT deposition, which freezes out the possible conversion to flat-lying geometries adopted particularly for NHCs with small side groups,[9,15−18] such as IMe.

Given that adsorption is a temperature-dependent process, thermodynamic considerations are essential to comprehensively identifying the adsorption properties of NHCs. To probe potential variations in the adsorption properties of IMe with temperature, we then deposited IMe onto Ag(111) held at RT. At very low coverage, no molecules are visible on Ag(111) terraces (Figure 5a), indicating a high mobility of IMe species under the scanning condition (78 K). More molecular deposition allows small self-assembled islands to be resolved (Figure 5b). However, the blurred perimeter suggests

https://doi.org/10.1021/acsnano.4c10942
ACS Nano 2024, 18, 32118−32125

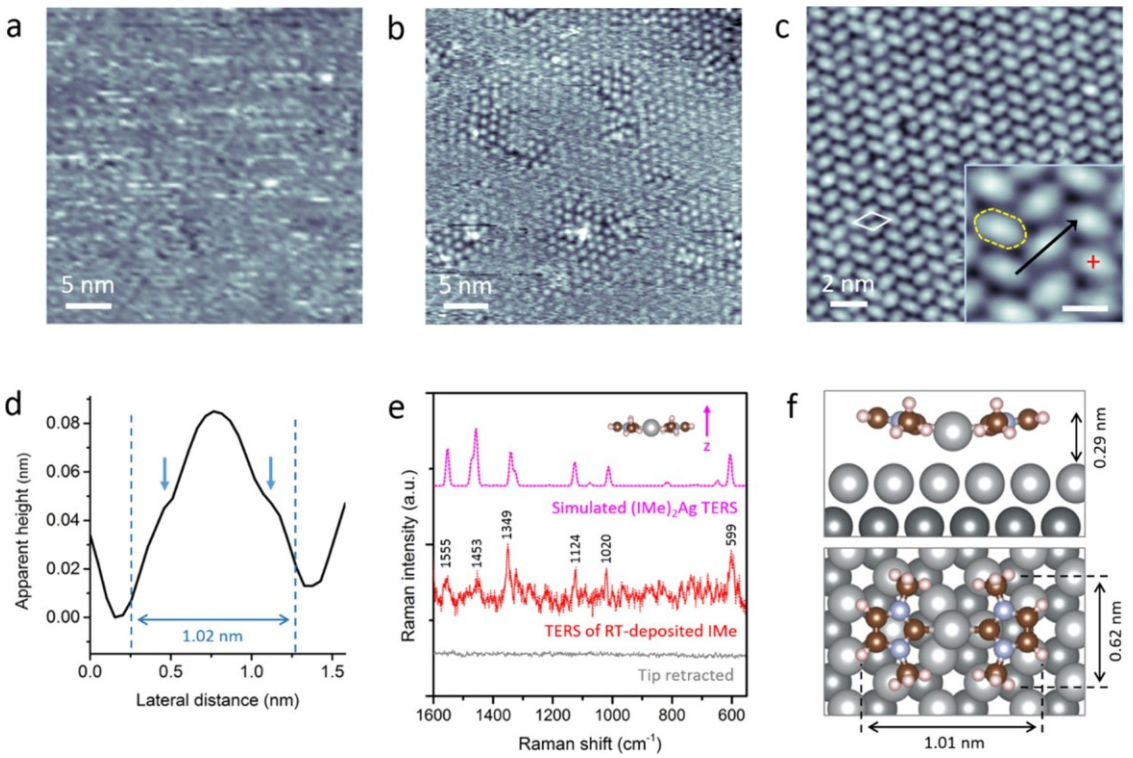

Figure 5. Chemically determining the geometry of IMe on Ag(111) deposited at room temperature. (a−c) STM topography of RT-deposited low-coverage (a), submonolayer (b), and full-monolayer (c) IMe molecules on Ag(111). Scale bar in (c) (inset): 1 nm. White rhombus in (c) marks the unit cell of the molecular pattern. (d) Height profile along the black arrow in (c). (e) TERS spectrum (red) acquired on the molecule marked by a plus in (c). Simulated TERS spectrum of $(IMe)_2Ag$ (magenta) is presented for comparison. (f) Optimized geometry of $(IMe)_2Ag$ complex on Ag(111). STM conditions: (a) − 1.5 V, 50 pA; (b) − 1.5 V, 27 pA; (c) − 1.5 V, 33 pA. TERS parameters: (e) 50 mV, 1.5 nA, 10 s.

instability and a dynamic nature of the molecular islands. Given the stability of LT-deposited IMe molecules under the same imaging condition (Figure 4a), this observation indicates a different adsorption geometry of RT-deposited IMe. By contrast, full-coverage IMe molecules were well resolved due to spatial constraint and were found to self-assemble into hexagonal close-packed lattices (Figure 5c).[15] Close-up inspection reveals a zigzag arrangement of flying shuttle-shaped protrusions (Figure 5c, inset), in sharp contrast to the round protrusions observed on LT-deposited IMe (Figure 4a). Notably, a bright dot is visible at the center of each protrusion, which is further confirmed by two symmetric shoulders in the height profile (Figure 5d, blue arrows) across a protrusion (Figure 5c, black arrow). Moreover, the height profile indicates a length of ~1.02 nm along the long axis of a protrusion. This measured size is much larger than that of a single IMe (0.62 nm, Figure 4d), hinting toward a dimer complex. Nevertheless, we cannot completely rule out the possibility of elongated protrusions being single IMe molecules due to the bias effect of STM topography.

TERS was then carried out to contribute to determining the adsorption geometry of RT-deposited IMe. Instead of a monomeric IMe, the resulting spectrum acquired on RT-deposited IMe (Figure 5e, red) is reproduced by the simulated spectrum of an $(IMe)_2Ag$ complex (see mode assignments in Figure S9). Specifically, the complex consists of two flat-lying IMe molecules that are covalently bound to a Ag adatom extracted from the Ag(111) substrate (i.e., IMe−Ag−IMe). Considering a free-space molecular complex used for the Raman calculation, the excellent agreement between the experimental and calculated TERS suggests a freestanding-like behavior of $(IMe)_2Ag$ complexes on Ag(111), consistent with the high mobility of RT-deposited IMe (Figure 5a,b). This observation can be rationalized by the calculated model shown in Figure 5f. The center Ag atom of the $(IMe)_2Ag$ complex is lifted off the surface (away from its equilibrium position by 0.29 nm) and thus behaves as a free adatom, in stark contrast to the surface Ag atoms that LT-deposited NHCs were found to bind to (Figures 2c and 4d).

The striking conversion from stable vertical IMe monomers deposited at LT to mobile flat-lying $(IMe)_2Ag$ complexes formed at RT indicates that the formation of the latter results from a thermal activation effect. It has been well documented that the structure of side groups plays a critical role in determining the binding mode of NHCs on metal surfaces.[9,16,17] Notably, the present study underlines temperature as another critical factor controlling NHC geometry and interfacial characteristics. From an application viewpoint, such insight into the temperature-dependent adsorption properties of NHCs contributes to understanding and tuning NHC modifications for device applications implemented in varied conditions.

CONCLUSIONS

This study demonstrated how STM-based TERS can chemically probe surface modifications at the single-molecule level by determining the structure and geometry of individual NHCs on a metal surface. We showed that, despite their topographic similarity in STM images, individual IPr and IMe molecules on Ag(111) can be identified by their spectroscopic signatures

https://doi.org/10.1021/acsnano.4c10942
ACS Nano 2024, 18, 32118−32125

obtained by single-molecule TERS. Furthermore, the temperature-dependent adsorption behaviors of NHCs can be determined via STM observations and TERS measurements combined with theoretical modeling. We found that LT-deposited IPr and IMe are stable on Ag(111) in the form of upright single molecules directly bound to surface sites. By contrast, RT-deposited IPr and IMe move readily on the surface due to the formation of highly mobile vertical IPr–Ag adatom complexes and quasi-freestanding flat-lying $(IMe)_2Ag$ complexes, respectively. These results deepen the understanding of NHC surface properties and phenomena at the most fundamental level. Lastly, we expect that the established methodology based on single-molecule vibrational spectroscopy will arouse extensive interest in NHC chemistry and be hopefully generalizable to the other fields in surface modification.

METHODS

Sample Growth. All experiments were carried out inside an ultrahigh vacuum (UHV, ~10^{-11} Torr) variable-temperature scanning tunneling microscopy (VT-STM) system (USM1400, UNISOKU Co., Ltd.) combined with a home-built optical setup. All sample growth was done in a preparation chamber (~10^{-10} Torr) which is separated from the STM chamber by a gate valve. Ag(111) foils grown on mica (Princeton Scientific) were prepared by repeated cycles of Ar^+ ion sputtering followed by annealing up to ~810 K. IPr and IMe molecules (>98% purity, Millipore-Sigma) were deposited via a standard Knudsen cell (ACME Technology Co., Ltd.) onto Ag(111) foils held at RT or LT. For LT deposition, we placed the Ag(111) substrate into the STM head and kept it for 1 h to reach 78 K. Then, we transferred the substrate to the UHV loadlock chamber, deposited NHCs from the K-cell onto the cold Ag(111) substrate and reinserted the substrate into the STM head. These procedures were finished within less than 2 min. Although we cannot exactly determine the temperature of the substrate during deposition, we estimate that it is below 150 K according to the observation of the maximum temperature (81 K) at the STM head after reinserting the cold sample.

STM and TERS Characterization. All STM and TERS characterizations were performed at liquid nitrogen temperature (78 K) using Ag tips prepared via an electrochemical etching process and cleaned in UHV by Ar^+ ion sputtering. All STM images were acquired in constant-current mode. A 561 nm solid-state CW laser (Lasos Laser GmbH) polarized parallel to the Ag tip was utilized as the incoming photon source for TERS experiments and the outgoing Raman signals were detected by an iso-plane SCT320 spectrograph (Princeton Instrument) coupled with a Princeton Instrument PIXIS 100 CCD. The detailed home-built optical setup has been pictured in our previous publication.[34,35] Significantly, in-vacuo lenses are positioned in close proximity to samples (and the tip) for maximum collection efficiency, which is crucial to chemically sensing single molecules. Specific STM imaging and TERS measurement parameters have been indicated in the main text (figure captions).

Computational Details. The VASP package[36] was employed to perform DFT calculations with the projector augmented wave pseudopotentials[37] and the Perdew–Burke–Ernzerhof generalized gradient approximation.[38] The van der Waals (vdW) interaction was included by using a nonlocal correlation functional.[39,40] An energy cutoff of 400 eV was used for the plane-wave basis set. Only the Γ-point in the Brillouin zone was used considering the large size of the supercell. We employed a four-layer slab with a (8 × 4) unit cell for the Ag(111) surface. The atoms in the top two layers were fully relaxed while the rest of the atoms were fixed in their equilibrium positions. The force convergence criterion for atomic relaxation is 0.01 eV/Å. The phonon modes of the free-space IPr and IMe were obtained by solving the eigenvalue problems of a dynamical or Hessian matrix based on density functional perturbation theory calculations.[41] Time-dependent DFT (TDDFT) calculations[42] were employed to determine the Raman intensity of the free-space IPr and IMe molecules.

ASSOCIATED CONTENT

Supporting Information

The Supporting Information is available free of charge at https://pubs.acs.org/doi/10.1021/acsnano.4c10942.

Bias dependence of the apparent height and lateral size of single IPr on Ag(111), optimized geometry of a free-space IPr coupled with a Ag atom, mode assignments and schematic atomic displacements of calculated Raman modes of IPr, IMe, and $(IMe)_2Ag$ complexes, surface selection rules and Raman simulation, TERS line scan, height measurements of IPr molecules on Ag(111), bias-dependent STM topography of single IMe molecules on Ag(111) (PDF)

AUTHOR INFORMATION

Corresponding Author

Nan Jiang − *Department of Chemistry, University of Illinois Chicago, Chicago, Illinois 60607, United States; Department of Physics, University of Illinois Chicago, Chicago, Illinois 60607, United States;* orcid.org/0000-0002-4570-180X; Email: njiang@uic.edu

Authors

Linfei Li − *Department of Chemistry, University of Illinois Chicago, Chicago, Illinois 60607, United States;* orcid.org/0000-0002-5217-3005

Sayantan Mahapatra − *Department of Chemistry, University of Illinois Chicago, Chicago, Illinois 60607, United States;* orcid.org/0000-0002-7332-196X

Jeremy F. Schultz − *Department of Chemistry, University of Illinois Chicago, Chicago, Illinois 60607, United States;* orcid.org/0000-0003-2231-6797

Xu Zhang − *Department of Physics and Astronomy, California State University, Northridge, Northridge, California 91330-8268, United States;* orcid.org/0000-0002-6491-3234

Complete contact information is available at: https://pubs.acs.org/10.1021/acsnano.4c10942

Author Contributions

L.L. and N.J. initiated the project; L.L. carried out the experiments and data analyses; X.Z. performed the theoretical calculations; L.L. authored the manuscript with inputs from J.F.S., S.M.; N.J. supervised the project.

Notes

The authors declare no competing financial interest.

ACKNOWLEDGMENTS

N.J. and L.L. acknowledge the support from the National Science Foundation DMR-2211474; N.J. and S.M. acknowledge the support from the National Science Foundation CHE-1944796; X.Z. acknowledges the support from the National Science Foundation DMR-1828019.

REFERENCES

(1) Bellotti, P.; Koy, M.; Hopkinson, M. N.; Glorius, F. Recent advances in the chemistry and applications of N-heterocyclic carbenes. *Nat. Rev. Chem.* 2021, *5* (10), 711–725.

(2) Zhukhovitskiy, A. V.; MacLeod, M. J.; Johnson, J. A. Carbene Ligands in Surface Chemistry: From Stabilization of Discrete

Elemental Allotropes to Modification of Nanoscale and Bulk Substrates. *Chem. Rev.* 2015, *115* (20), 11503−11532.
(3) Smith, C. A.; Narouz, M. R.; Lummis, P. A.; Singh, I.; Nazemi, A.; Li, C. H.; Crudden, C. M. N. Heterocyclic Carbenes in Materials Chemistry. *Chem. Rev.* 2019, *119* (8), 4986−5056.
(4) Koy, M.; Bellotti, P.; Das, M.; Glorius, F. N-Heterocyclic carbenes as tunable ligands for catalytic metal surfaces. *Nat. Catal.* 2021, *4* (5), 352−363.
(5) Zhukhovitskiy, A. V.; Mavros, M. G.; Van Voorhis, T.; Johnson, J. A. Addressable Carbene Anchors for Gold Surfaces. *J. Am. Chem. Soc.* 2013, *135* (20), 7418−7421.
(6) Crudden, C. M.; Horton, J. H.; Ebralidze, I. I.; Zenkina, O. V.; McLean, A. B.; Drevniok, B.; She, Z.; Kraatz, H. B.; Mosey, N. J.; Seki, T.; Keske, E. C.; Leake, J. D.; Rousina-Webb, A.; Wu, G. Ultra stable self-assembled monolayers of N-heterocyclic carbenes on gold. *Nat. Chem.* 2014, *6* (5), 409−414.
(7) Wang, G. Q.; Ruhling, A.; Amirjalayer, S.; Knor, M.; Ernst, J. B.; Richter, C.; Gao, H. J.; Timmer, A.; Gao, H. Y.; Doltsinis, N. L.; Glorius, F.; Fuchs, H. Ballbot-type motion of N-heterocyclic carbenes on gold surfaces. *Nat. Chem.* 2017, *9* (2), 152−156.
(8) Franz, M.; Chandola, S.; Koy, M.; Zielinski, R.; Aldahhak, H.; Das, M.; Freitag, M.; Gerstmann, U.; Liebig, D.; Hoffmann, A. K.; Rosin, M.; Schmidt, W. G.; Hogan, C.; Glorius, F.; Esser, N.; Dahne, M. Controlled growth of ordered monolayers of N-heterocyclic carbenes on silicon. *Nat. Chem.* 2021, *13* (9), 828−835.
(9) Inayeh, A.; Groome, R. R. K.; Singh, I.; Veinot, A. J.; de Lima, F. C.; Miwa, R. H.; Crudden, C. M.; McLean, A. B. Self-assembly of N-heterocyclic carbenes on Au(111). *Nat. Commun.* 2021, *12* (1), No. 4034.
(10) Navarro, J. J.; Das, M.; Tosoni, S.; Landwehr, F.; Bruce, J. P.; Heyde, M.; Pacchioni, G.; Glorius, F.; Roldan Cuenya, B. Covalent Adsorption of N-Heterocyclic Carbenes on a Copper Oxide Surface. *J. Am. Chem. Soc.* 2022, *144* (36), 16267−16271.
(11) Navarro, J. J.; Das, M.; Tosoni, S.; Landwehr, F.; Koy, M.; Heyde, M.; Pacchioni, G.; Glorius, F.; Roldan Cuenya, B. Growth of N-Heterocyclic Carbene Assemblies on Cu(100) and Cu(111): From Single Molecules to Magic-Number Islands. *Angew. Chem., Int. Ed.* 2022, *61* (30), No. e202202127.
(12) Qie, B.; Wang, Z.; Jiang, J.; Zhang, Z.; Jacobse, P. H.; Lu, J.; Li, X.; Liu, F.; Alexandrova, A. N.; Louie, S. G.; et al. Synthesis and characterization of low-dimensional N-heterocyclic carbene lattices. *Science* 2024, *384* (6698), 895−901.
(13) DeJesus, J. F.; Trujillo, M. J.; Camden, J. P.; Jenkins, D. M. N-Heterocyclic Carbenes as a Robust Platform for Surface-Enhanced Raman Spectroscopy. *J. Am. Chem. Soc.* 2018, *140* (4), 1247−1250.
(14) Trujillo, M. J.; Strausser, S. L.; Becca, J. C.; DeJesus, J. F.; Jensen, L.; Jenkins, D. M.; Camden, J. P. Using SERS To Understand the Binding of N-Heterocyclic Carbenes to Gold Surfaces. *J. Phys. Chem. Lett.* 2018, *9* (23), 6779−6785.
(15) Jiang, L.; Zhang, B. D.; Médard, G.; Seitsonen, A. P.; Haag, F.; Allegretti, F.; Reichert, J.; Kuster, B.; Barth, J. V.; Papageorgiou, A. C. N-Heterocyclic carbenes on close-packed coinage metal surfaces: bis-carbene metal adatom bonding scheme of monolayer films on Au, Ag and Cu. *Chem. Sci.* 2017, *8* (12), 8301−8308.
(16) Bakker, A.; Timmer, A.; Kolodzeiski, E.; Freitag, M.; Gao, H. Y.; Mönig, H.; Amirjalayer, S.; Glorius, F.; Fuchs, H. Elucidating the Binding Modes of N-Heterocyclic Carbenes on a Gold Surface. *J. Am. Chem. Soc.* 2018, *140* (38), 11889−11892.
(17) Lovat, G.; Doud, E. A.; Lu, D. Y.; Kladnik, G.; Inkpen, M. S.; Steigerwald, M. L.; Cvetko, D.; Hybertsen, M. S.; Morgante, A.; Roy, X.; Venkataraman, L. Determination of the structure and geometry of N-heterocyclic carbenes on Au(111) using high-resolution spectroscopy. *Chem. Sci.* 2019, *10* (3), 930−935.
(18) Thimes, R. L.; Santos, A. V. B.; Chen, R.; Kaur, G.; Jensen, L.; Jenkins, D. M.; Camden, J. P. Using Surface-Enhanced Raman Spectroscopy to Unravel the Wingtip-Dependent Orientation of N-Heterocyclic Carbenes on Gold Nanoparticles. *J. Phys. Chem. Lett.* 2023, *14* (18), 4219−4224.
(19) Chowdhury, S.; Hu, G.; Jensen, I. M.; Santos, A. V. B.; Jenkins, D. M.; Jensen, L.; Camden, J. P. Vibrational Mode Assignment of Diisopropyl Benzimidazolium N-Heterocyclic Carbenes on Gold. *J. Phys. Chem. C* 2024, *128* (32), 13550−13557.
(20) Jiang, N.; Foley, E. T.; Klingsporn, J. M.; Sonntag, M. D.; Valley, N. A.; Dieringer, J. A.; Seideman, T.; Schatz, G. C.; Hersam, M. C.; Van Duyne, R. P. Observation of Multiple Vibrational Modes in Ultrahigh Vacuum Tip-Enhanced Raman Spectroscopy Combined with Molecular-Resolution Scanning Tunneling Microscopy. *Nano Lett.* 2012, *12*, 5061−5067.
(21) Mahapatra, S.; Ning, Y.; Schultz, J. F.; Li, L.; Zhang, J.-L.; Jiang, N. Angstrom Scale Chemical Analysis of Metal Supported *Trans*- and *Cis*-Regioisomers by Ultrahigh Vacuum Tip-Enhanced Raman Mapping. *Nano Lett.* 2019, *19*, 3267−3272.
(22) Pozzi, E. A.; Goubert, G.; Chiang, N. H.; Jiang, N.; Chapman, C. T.; McAnally, M. O.; Henry, A. I.; Seideman, T.; Schatz, G. C.; Hersam, M. C.; Van Duyne, R. P. Ultrahigh-Vacuum Tip-Enhanced Raman Spectroscopy. *Chem. Rev.* 2017, *117* (7), 4961−4982.
(23) Li, L. F.; Schultz, J. F.; Mahapatra, S.; Liu, X. L.; Shaw, C.; Zhang, X.; Hersam, M. C.; Jiang, N. Angstrom-Scale Spectroscopic Visualization of Interfacial Interactions in an Organic/Borophene Vertical Heterostructure. *J. Am. Chem. Soc.* 2021, *143* (38), 15624−15634.
(24) Zhang, R.; Zhang, Y.; Dong, Z. C.; Jiang, S.; Zhang, C.; Chen, L. G.; Zhang, L.; Liao, Y.; Aizpurua, J.; Luo, Y.; Yang, J. L.; Hou, J. G. Chemical mapping of a single molecule by plasmon-enhanced Raman scattering. *Nature* 2013, *498* (7452), 82−86.
(25) Lee, J.; Crampton, K. T.; Tallarida, N.; Apkarian, V. A. Visualizing vibrational normal modes of a single molecule with atomically confined light. *Nature* 2019, *568* (7750), 78−82.
(26) Jaculbia, R. B.; Imada, H.; Miwa, K.; Iwasa, T.; Takenaka, M.; Yang, B.; Kazuma, E.; Hayazawa, N.; Taketsugu, T.; Kim, Y. Single-molecule resonance Raman effect in a plasmonic nanocavity. *Nat. Nanotechnol.* 2020, *15* (2), 105−110.
(27) Li, L.; Schultz, J. F.; Mahapatra, S.; Liu, X.; Zhang, X.; Hersam, M. C.; Jiang, N. Atomic-Scale Insights into the Interlayer Characteristics and Oxygen Reactivity of Bilayer Borophene. *Angew. Chem. Int. Ed.* 2023, *62*, e202306590.
(28) Jiang, S.; Zhang, Y.; Zhang, R.; Hu, C. R.; Liao, M. H.; Luo, Y.; Yang, J. L.; Dong, Z. C.; Hou, J. G. Distinguishing adjacent molecules on a surface using plasmon-enhanced Raman scattering. *Nat. Nanotechnol.* 2015, *10* (10), 865−869.
(29) Li, L. F.; Schultz, J. F.; Mahapatra, S.; Lu, Z. Y.; Zhang, X.; Jiang, N. Chemically identifying single adatoms with single-bond sensitivity during oxidation reactions of borophene. *Nat. Commun.* 2022, *13* (1), No. 1796.
(30) Cai, Z. F.; Merino, J. P.; Fang, W.; Kumar, N.; Richardson, J. O.; De Feyter, S.; Zenobi, R. Molecular-Level Insights on Reactive Arrangement in On-Surface Photocatalytic Coupling Reactions Using Tip-Enhanced Raman Spectroscopy. *J. Am. Chem. Soc.* 2022, *144* (1), 538−546.
(31) Jiang, N.; Chiang, N. H.; Madison, L. R.; Pozzi, E. A.; Wasielewski, M. R.; Seideman, T.; Ratner, M. A.; Hersam, M. C.; Schatz, G. C.; Van Duyne, R. P. Nanoscale Chemical Imaging of a Dynamic Molecular Phase Boundary with Ultrahigh Vacuum Tip-Enhanced Raman Spectroscopy. *Nano Lett.* 2016, *16* (6), 3898−3904.
(32) Xu, J. Y.; Zhu, X.; Tan, S. J.; Zhang, Y.; Li, B.; Tian, Y. Z.; Shan, H.; Cui, X. F.; Zhao, A. D.; Dong, Z. C.; Yang, J. L.; Luo, Y.; Wang, B.; Hou, J. G. Determining structural and chemical heterogeneities of surface species at the single-bond limit. *Science* 2021, *371* (6531), 818−822.
(33) Moskovits, M. Surface selection rules. *J. Chem. Phys.* 1982, *77* (9), 4408−4416.
(34) Whiteman, P. J.; Schultz, J. F.; Porach, Z. D.; Chen, H. N.; Jiang, N. Dual Binding Configurations of Subphthalocyanine on Ag(100) Substrate Characterized by, Scanning Tunneling Microscopy, Tip-Enhanced Raman Spectroscopy, and Density Functional Theory. *J. Phys. Chem. C* 2018, *122* (10), 5489−5495.

https://doi.org/10.1021/acsnano.4c10942
ACS Nano 2024, 18, 32118−32125

(35) Mahapatra, S.; Li, L. F.; Schultz, J. F.; Jiang, N. Methods to fabricate and recycle plasmonic probes for ultrahigh vacuum scanning tunneling microscopy-based tip-enhanced Raman spectroscopy. *J. Raman Spectrosc.* 2021, *52* (2), 573–580.
(36) Kresse, G.; Furthmuller, J. Efficient iterative schemes for ab initio total-energy calculations using a plane-wave basis set. *Phys. Rev. B* 1996, *54* (16), 11169–11186.
(37) Blöchl, P. E. Projector Augmented-Wave Method. *Phys. Rev. B* 1994, *50* (24), 17953–17979.
(38) Perdew, J. P.; Burke, K.; Ernzerhof, M. Generalized gradient approximation made simple. *Phys. Rev. Lett.* 1996, *77* (18), 3865–3868.
(39) Dion, M.; Rydberg, H.; Schroder, E.; Langreth, D. C.; Lundqvist, B. I. Van der Waals density functional for general geometries. *Phys. Rev. Lett.* 2004, *92* (24), No. 246401.
(40) Klimeš, J.; Bowler, D. R.; Michaelides, A. Van der Waals density functionals applied to solids. *Phys. Rev. B* 2011, *83* (19), No. 195131.
(41) Baroni, S.; de Gironcoli, S.; Dal Corso, A.; Giannozzi, P. Phonons and related crystal properties from density-functional perturbation theory. *Rev. Mod. Phys.* 2001, *73* (2), 515–562.
(42) Zhang, X. Large-scale ab initio calculations of Raman scattering spectra within time-dependent density functional perturbation theory. *J. Chem. Phys.* 2018, *148* (24), No. 244103.

https://doi.org/10.1021/acsnano.4c10942
ACS Nano 2024, 18, 32118–32125